Electrical Transport Property in van der Waals Insulator $CrGeTe_3$ under Extremely High Pressure up to 52 GPa

*Ryo Matsumoto[1], Sayaka Yamamoto[1,2], Kensei Terashima[1], Kazuki Yamane[1,2], Yoshihiko Takano[1,2]

[1]*Research Center for Materials Nanoarchitectonics (MANA), National Institute for Materials Science, Tsukuba, Ibaraki 305-0047, Japan*

[2]*Graduate School of Pure and Applied Sciences, University of Tsukuba, 1-1-1 Tennodai, Tsukuba, Ibaraki 305-8577, Japan*

**Corresponding author; Email: matsumoto.ryo@nims.go.jp*

Abstract

Layered ternary chalcogenide $CrGeTe_3$ has attracted considerable interest as a two-dimensional van der Waals magnet. The application of high pressures induces unique property modifications, such as a drastic increase in the Curie temperature to a value close to room temperature. In this study, the electrical transport properties of $CrGeTe_3$ were investigated under extremely high pressures up to 52 GPa to understand the physical properties of the high-pressure phase further, particularly the appearance of superconductivity. The temperature dependences of the resistance, Hall effect, and magnetoresistance at high pressures were measured using an originally designed diamond anvil cell. The structural phase transitions from the *R-3* to *R3* structure and amorphization are investigated via in situ Raman spectroscopy and X-ray diffraction at high pressures. Unlike in $CrSiTe_3$, the emergence of superconductivity in $CrGeTe_3$ in the high-pressure phase is not observed up to 52 GPa. Amorphization is the possible main reason for the absence of superconductivity in $CrGeTe_3$.

1. Introduction

Two-dimensional (2D) van der Waals (2D-vdW) materials with layered structures have received considerable attention because they are a promising platform for examining the abundant physical phenomena available based on a tunable film thickness [1-5]. Among these materials, layered $Cr(Si.Ge)Te_3$ is a ferromagnetic insulator that has recently attracted interest as a low-dimensional magnetic material [6,7]. At ambient pressure, $CrSiTe_3$ exhibits a paramagnetic-to-ferromagnetic phase transition at a Curie temperature (T_C) of 32 K [8]. Interestingly, T_C drastically increases as pressure is applied, reaching 138 K at 7.8 GPa, from 36 K at 4.6 GPa [9]. At higher pressure, $CrSiTe_3$ undergoes a structural phase transition from the *R-3* to *R3* space group and an insulator-to-metal transition (IMT) [10]. Moreover, superconductivity at the transition temperature of 3 K has been reported for *R3* structures. Ferromagnetism vanishes during the structural phase transition, and superconductivity appears instead. Further investigation of the physical properties under high pressures is expected in this system because several 2D-vdW materials exhibit more interesting functionalities at higher pressures, as 2H-TaS_2 shows a record-high T_c of 16 K above 150 GPa [11].

Isostructural $CrGeTe_3$ is also a 2D-vdW ferromagnetic insulator with a T_C of 65 K, which is twice that of $CrSiTe_3$ at ambient pressure [12,13]. The higher T_C motivated us to reveal several functionalities, such as the drastic enhancement in T_C via the intercalation of organic ions into the layered structure [14]. The application of high pressures to $CrGeTe_3$ has also been reported to enhance the magnetic properties, for example, a drastic enhancement in T_c up to 250 K under 9 GPa [15] and the control of magnetic anisotropy [16]. Based on the electrical and structural properties, an IMT at 11 GPa [15] and a structural phase transition from *R-3* to *R3* at a high pressure of 18 GPa have been reported [17]. A unique crystalline-to-amorphous transition occurs at higher pressure [17], as observed in the case of $CrSiTe_3$ [18]. Raman observations and first-principles phonon dispersion calculations indicate that pressure-induced phonon softening occurs in $CrGeTe_3$ [19], which is preferred for superconductivity [20-22]. However, electrical transport properties under pressure have only been reported below 11 GPa [15]. Further investigation under higher pressures will accelerate the understanding of the physical properties of the crystalline *R3* and amorphous phases in this system, including pressure-induced superconductivity.

In this study, we evaluate the electrical transport properties, including the temperature-dependent resistance, Hall effect, and magnetoresistance (MR), of $CrGeTe_3$ single crystals under extremely high pressures up to 52 GPa using a custom-designed diamond anvil cell (DAC). Furthermore, in situ Raman spectroscopy measurements and X-ray diffraction (XRD) analyses are performed under pressure to investigate the structural phase transition and amorphization. In contrast to $GeSiTe_3$, pressure-induced superconductivity is not observed at pressures up to 52 GPa for $CrGeTe_3$.

2. Experimental Procedures

Single-crystalline $CrGeTe_3$ was grown using the following procedure: The starting materials of elemental Cr, Ge, and Te with molar ratio of 1:1:36 were sealed inside an evacuated quartz tube. The ampoule was heated at 700°C for 20 days and then slowly cooled to 500°C over a period of 1.5 days, and then subjected to furnace cooling. The crystal structures of the resultant samples were analyzed using XRD using a MiniFlex 600 diffractometer (Rigaku) with Cu Kα radiation (λ = 1.5418

Å). The VESTA software package was used to visualize crystal structures [23]. The crystal composition was investigated using energy-dispersive X-ray spectroscopy (EDX) with a JSM-6010LA scanning electron microscope (JEOL). The temperature dependence of the magnetization of the obtained crystals was evaluated using a magnetic property measurement system (Quantum Design). Electrical transport measurements were obtained at high pressures via the standard four-probe method using a custom-designed DAC [24-26] set within a physical property measurement system with a superconducting magnet (Quantum Design). Cubic boron nitride powder was used as a pressure-transmitting medium. The applied pressures were estimated from the fluorescence emitted by ruby powders [27] and from the Raman spectrum acquired from a culet of the upper diamond anvil [28], which was obtained using an inVia Raman Microscope (Renishaw plc). These measurements were performed simultaneously with high-pressure in situ Raman spectroscopy acquisitions of the sample. The XRD patterns at high pressures were obtained in a DAC by utilizing synchrotron radiation at the AR-NE1A beamline of the Photon Factory (PF) situated at the High Energy Accelerator Research Organization (KEK). The X-ray beam was monochromatized to an energy of 30 keV (λ = 0.41815 Å) and introduced to the sample in the DAC through a collimator with a diameter of 50 μm. The obtained XRD patterns were subsequently integrated into a one-dimensional profile using an IPAnalyzer [29]. Cubic BN powder was also used as the pressure-transmitting medium in the XRD measurements under high pressures.

3. Results and Discussion

Figure 1 (a) shows the XRD pattern of a single crystal of $CrGeTe_3$. The inset displays a typical micrograph and the crystal structure with the definitions of the *a*, *b*, and *c* axes. The well-developed plate-like morphology of $CrGeTe_3$ is apparent in the images. The pattern including only the (003*n*) diffraction peaks indicates a highly *c*-axis-oriented crystal. The elemental composition is determined to be Cr:Ge:Te = 1.9:2:6.0 from the EDX analysis by normalizing to Ge = 2. Figures 1 (b) and 1 (c) show the temperature dependence of the magnetization M and resistivity ρ of the $CrGeTe_3$ single crystal at ambient pressure. Using the derivative of the magnetization dM/dT and the Arrhenius relationship, $\rho = \rho_0 \exp(E_a/k_B T)$, where ρ_0 is the residual resistivity, E_a is the activation energy, k_B is the Boltzmann constant, and T is the temperature, the T_C and activation energy are determined to be 65 K and 0.24 eV, respectively. The observed magnetic and electric properties at ambient pressure are consistent with the previously reported values [30].

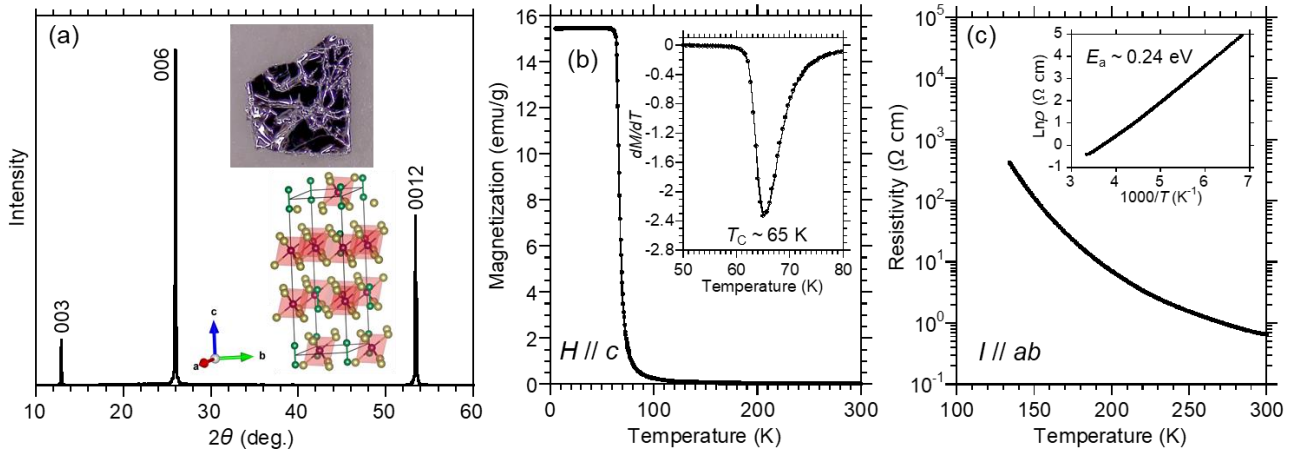

Fig. 1. (Color online) Characterization of the obtained $CrGeTe_3$ single crystal. (a) XRD pattern. Inset: typical micrograph and crystal structure. (b) Temperature dependence of magnetization and the derivative *dM/dT* as an inset. (c) Temperature dependence of resistivity and Arrhenius plot (inset).

Figures 2 (a) and (b) show the results of Hall measurements at 300 K with the application of various pressures to the $CrGeTe_3$ single crystal. The slope of the Hall voltage is positive at each pressure, indicating p-type characteristics. The Hall voltage drastically decreases with increasing pressure up to 3.2 GPa. The carrier concentration of the sample is calculated from the slope of the Hall voltage vs. the magnetic field strength using the formula $V_H/I = H/ned$, where V_H is the Hall voltage, I is the current, n is the number of carriers, e is the elementary charge, H is the magnetic field strength, and d is the sample thickness. Figure 2 (c) shows the applied pressure dependence of the carrier concentration in the $CrGeTe_3$ single crystal at various pressures. The carrier concentration at the lowest pressure of 0.44 GPa is 1.3×10^{18} cm^{-3}, indicating that the sample shows a semiconducting character under these conditions. The application of pressure enhances the carrier concentration to values on the order of at least 10^{21} cm^{-3}.

Figure 2(d) shows the magnetic field dependence of the MR ratio $(R-R_0)/R_0$ at various pressures, where R_0 is the resistance at zero-field of the $CrGeTe_3$ single crystal. The MR ratio decreases as the pressure increased from 0.90 to 1.8 GPa. The sign of the MR ratio switches from negative to positive between 1.8 and 3.2 GPa, corresponding to a spin-reorientation transition from the *c* axis to the *ab* plane [31]. In addition, the magnitude of the MR ratio decreases at 3.2 GPa. The sign of the MR again reverses, becoming negative at 4.3 GPa, and its magnitude at this pressure is comparable to that at 1.8 GPa. With compression up to 13 GPa, the magnitude of the MR ratio increases slightly without any further changes in its sign. Recent high-pressure magnetic measurements have indicated that the magnetization drastically decreases as the pressure is increased up to 4.0 GPa, before increasing again with an increase in pressure from 5.0 to 7.3 GPa [15]. Further investigation of the origin of the magnetic transition at approximately 4.0 GPa should prove to be an interesting topic for future studies.

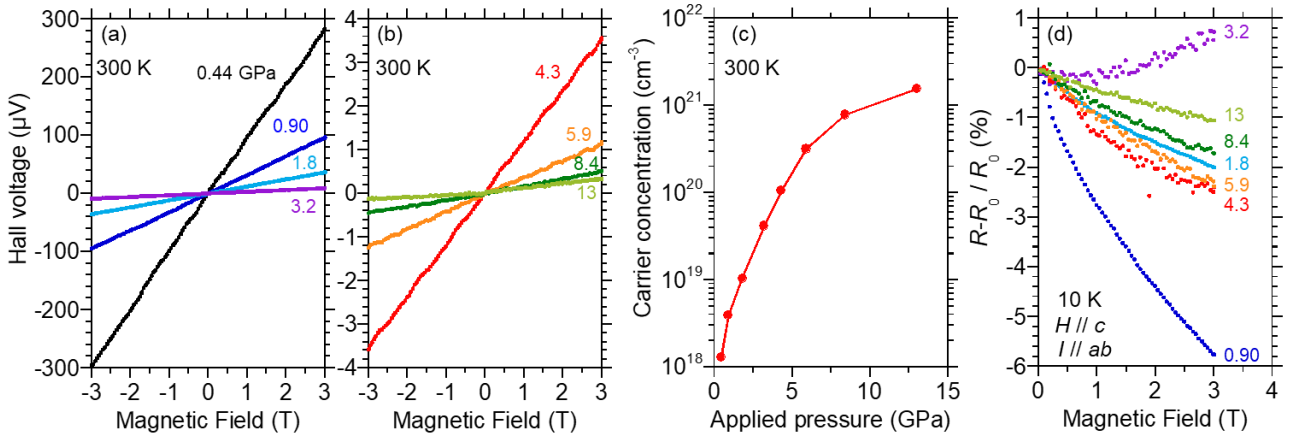

Fig. 2. (Color online) Hall effect at 300 K in the $CrGeTe_3$ single crystal under various pressures in the ranges of (a) 0.44–3.2 GPa and (b) 4.3–13 GPa. (c) Applied pressure dependence of the carrier concentration. (d) Magnetic field dependence of the MR ratio at pressures in the range

of 0.90–13 GPa.

Figure 3 (a) shows the temperature dependence of the resistance of the $CrGeTe_3$ single crystal at pressures ranging from 0.44 to 18 GPa. At 0.90 GPa, the curve of resistance exhibits two hump-like structures at approximately 80 K (hump 1) and 190 K (hump 2). As shown in the logarithmic scale of Fig. 3 (b), hump 1 gradually disappears, and the temperature of hump 2 increases with the applied pressure. According to a previous report [15], the hump in the resistance curve is a possible signature of magnetic transition. At 3.2 GPa, hump 2 appears at approximately 250 K, which is slightly higher than that reported previously [15]. The resistance at 300 K decreases monotonically when the pressure increases, as shown in Fig. 3 (c). In total, the resistance of the $CrGeTe_3$ single crystal at 300 K decreases by more than two orders of magnitude as the pressure increases from ambient pressure to 18 GPa. The inset in Fig. 3 (c) shows the temperature dependence of the resistance at 3.2 GPa with a standard power-law fit, $R(T) = R_0 + AT^n$, where R_0 is the residual resistance, A is a characteristic constant, and T is the temperature. The fitting results yield the parameters of $n = 2.58(1)$, $R_0 = 0.30(3)$ Ω, and $A = 1.15(5)\times10^{-5}$ Ω/K^2. This well-fitted feature indicates that an IMT occurred at 3.2 GPa, which is slightly lower than the previously reported IMT pressure [15]. The drastic reduction in resistance and IMT with the application of pressure is consistent with the increasing carrier concentration.

Figure 3 (d) shows the temperature dependence of the resistance of the $CrGeTe_3$ single crystal at high pressures ranging from 15 to 52 GPa. The decrease in the resistance with increasing pressure continues up to 52 GPa. In the case of $CrSiTe_3$, the original *R-3* structure undergo a high-pressure phase of the *R3* structure, and pressure-induced superconductivity appears above 9 GPa. Although a similar pathway for the structural phase transition from *R-3* to *R3* above 18 GPa has been reported for $CrGeTe_3$ [17], pressure-induced superconductivity is absent at the pressure. In addition, superconductivity has been never observed between 23 and 52 GPa, which is the amorphous region of $CrGeTe_3$ [17].

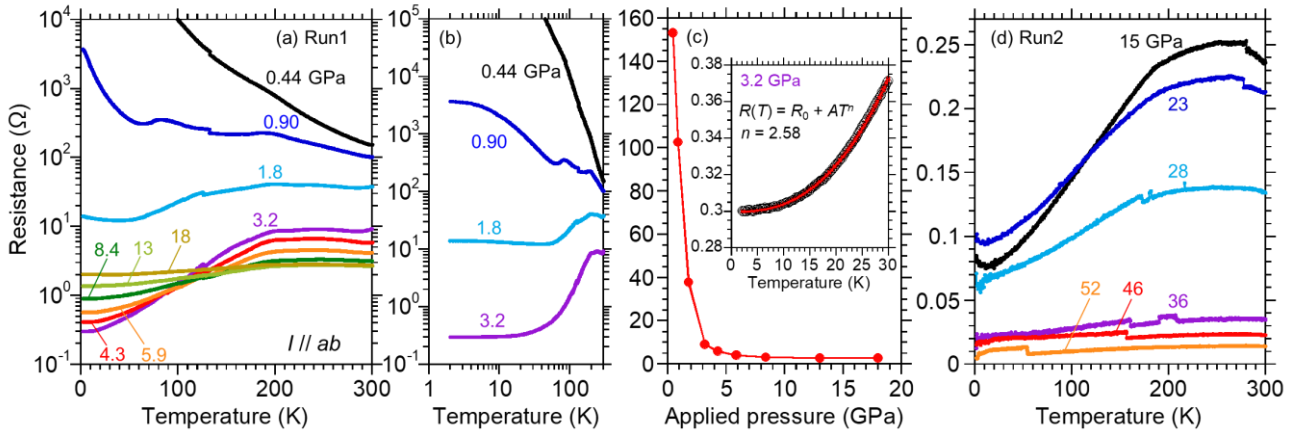

Fig. 3. (Color online) Temperature dependence of the resistance of the $CrGeTe_3$ single crystal at high pressures in the ranges of (a,b) 0.44–18 GPa and (d) 15–52 GPa. (c) Applied pressure dependence of the resistance at 300 K. The inset is the temperature dependence of the resistance at 3.2 GPa with power-law fitting.

Structural analyses using in situ Raman spectroscopy and XRD under pressure were conducted to determine the absence of superconductivity in $CrGeTe_3$. Figure 4 (a) shows the Raman spectra of the $CrGeTe_3$ single crystal under various pressures. At ambient pressure, five Raman-active modes are identified at different wavenumbers: 109.6 cm^{-1} (E_g^3), 135.7 cm^{-1} (A_g^1), 211.9 cm^{-1} (E_g^4), 232.2 cm^{-1} (E_g^5), and 291.0 cm^{-1} (A_g^2). These assignments are based on previously reported spectroscopic studies [32,33]. A small unidentified peak, labeled with an asterisk in Fig. 4 (a), appears between the A_g^1 and E_g^3 modes with slight compression. All the observed peaks, apart from the E_g^4 mode, gradually shifts to higher wavenumbers as the pressure increases to 11 GPa via phonon hardening without a structural phase transition, as shown in Fig. 4 (b). The peak corresponding to the E_g^4 mode disappears at approximately 4 GPa. However, all the Raman peaks disappear at pressures higher than 15 GPa, corresponding to a pressure-induced crystalline-to-crystalline transition from the *R*-3 to *R*3 structure, as reported in the literature [19]. With a further increase in the pressure to 52 GPa, no new peaks appear in the spectrum.

Although an emergence of pressure-induced superconductivity in $CrGeTe_3$ is expected in the *R*3 structure, considering the case of $CrSiTe_3$, it is absent even above the critical pressure of the structural transition. To answer this question, amorphization was investigated by comparing the Raman spectra before and after compression. Figure 4 (c) shows a comparison of the Raman spectra of ambient $CrGeTe_3$ single crystals and recovered samples from various maximum pressures. The sharp peaks observed at ambient pressure disappear in the recovered sample from 52 and 39 GPa, and broad humps are observed. Peak broadening after decompression is a signature of pressure-induced amorphization, as seen in phase-change memory materials, such as $Ge_2Sb_2Te_5$, $GeSb_2Te_4$, and $SnSb_2Te_4$ [34]. The recovered sample from 20 GPa, whose pressure is close to the critical pressure of the *R-3* to *R3* transition, shows the peak broadening, although the peak positions are almost reproduced. The sample recovered from 5.6 GPa exhibits relatively sharp peaks, although the overall shape of the spectrum is different from that recorded at ambient pressure without compression. The irreversibility of the Raman spectra suggests that pressure-induced amorphization progresses gradually with increasing pressure.

Figure 4 (d) shows the XRD patterns of the $CrGeTe_3$ single crystal at 1.6 GPa and the sample recovered from 22.6 GPa. The insets display Debye–Scherrer diffraction peaks. All the observed diffraction peaks at 1.6 GPa correspond to the trigonal *R-3* structure, except for the peaks from cubic BN, which is a pressure-transmitting medium. The Debye–Scherrer ring at 1.6 GPa exhibits spot-like diffractions, reflecting a single-crystalline feature. In contrast, the spot-like diffractions disappear, and only broadened rings are observed in the recovered sample from 22.6 GPa. The irreversibility of the XRD pattern also indicates amorphization around the critical pressure of structural transition in $CrGeTe_3$ [17]. As $CrGeTe_3$ requires a higher pressure to undergo the *R3* structure than $CrSiTe_3$, the absence of superconductivity could be related to progressive amorphization under high-pressure conditions.

One of the possibilities for inducing the absence of superconductivity in $CrGeTe_3$ based on the aforementioned scenario is the deterrence of amorphization under high pressures. In our configuration of DAC, a solid pressure-transmitting medium is used, which provides a nonhydrostatic pressure. The typical signature of the nonhydrostatic pressure is observed a broadened ruby fluorescence as shown

in Fig. S1 [35]. Nonhydrostatic pressure creates distortion stress and affects the physical properties of the crystal [36]. The differences between the measured resistances and the absence of superconductivity could possibly be the result of the uniaxial nature of the applied pressure, because 2D materials are sensitive to strain, as has been observed for graphene [37], transition metal dichalcogenides [38], and black phosphorous [39]. In future study, the application of hydrostatic pressure using a liquid pressure-transmitting medium is expected to induce superconductivity in $CrGeTe_3$. In addition, the irreversible change in crystal structure after compression is interesting because of the possibility of quenching the high-pressure phase under ambient conditions. In particular, a drastic enhancement in T_C close to room temperature has been reported with the application of pressure [15]. Physical property measurements of the recovered amorphous sample are important for the practical use of magnetic materials.

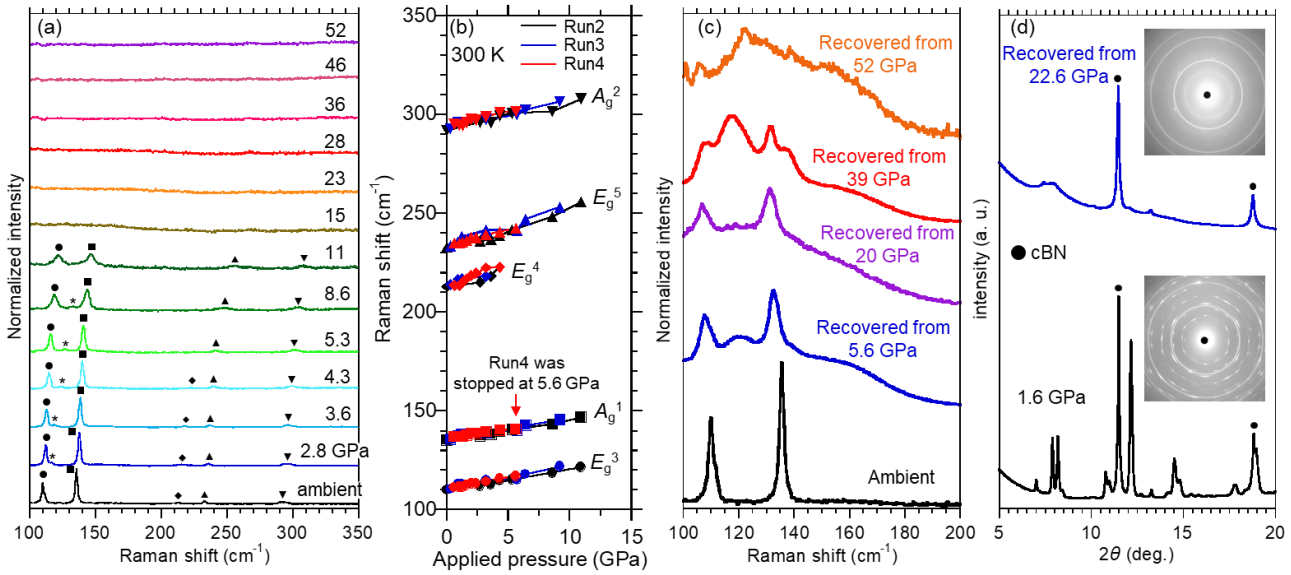

Fig. 4. (Color online) (a) Raman spectra of the $CrGeTe_3$ single crystal at various pressures. (b) Applied pressure dependence of the peak positions of the Raman modes. (c) Comparison of Raman spectra from the original $CrGeTe_3$ and the recovered sample after compression under various pressures. (d) XRD patterns from the $CrGeTe_3$ single crystal at 1.6 GPa and the recovered sample from 22.6 GPa. The insets are Debye–Scherrer diffraction rings.

4. Conclusion

We performed electrical transport measurements and observed the resistance, Hall effect, and MR of $CrGeTe_3$ single crystals at high pressures. The carrier concentration increased from ~10^{18} cm^{-3} at 0.44 GPa to 10^{21} cm^{-3} at 13 GPa. The sign of the MR ratio switched twice: from negative to positive at 3.2 GPa and from positive to negative at 4.3 GPa. A drastic reduction in the resistance with IMT was observed at approximately 3.2 GPa. In transport measurements, superconductivity observed for $CrSiTe_3$ was not observed even in the high-pressure phase of the *R*3 structure. The in situ Raman analysis of the sample at high pressures revealed a crystalline-to-crystalline transition from the *R*-3 to *R*3 space group, similar to superconducting $CrSiTe_3$. The irreversibility of the Raman spectrum and XRD pattern suggests that the $CrGeTe_3$ single crystal gradually transformed into an amorphous phase with increasing pressure. We hypothesized that this amorphization would impede the emergence of

superconductivity in $CrGeTe_3$. In a future study, the measurement of the physical properties of the recovered sample will be interesting from the viewpoint of the possibility of quenching the high-pressure phase.

Acknowledgment

This study was partly supported by the JST-Mirai Program Grant Number JPMJMI17A2 and JSPS KAKENHI Grant Number 23K13549. The fabrication of the diamond electrodes was partially supported by the NIMS Nanofabrication Platform in the Nanotechnology Platform Project, sponsored by the Ministry of Education, Culture, Sports, Science, and Technology (MEXT), Japan. The synchrotron X-ray experiments were performed at AR-NE1A (KEK-PF) under the approval of Proposal No. 2022G049 with the support of Dr. Y. Shibazaki (KEK).

References

[1] K. S. Novoselov, A. K. Geim, S. V. Morozov, D. Jiang, Y. Zhang, S. V. Dubonos, I. V. Grigorieva, and A. A. Firsov, Electric field effect in atomically thin carbon films, Science **306**, 666 (2004).

[2] K. F. Mak, C. Lee, J. Hone, J. Shan, and T. F. Heinz, Atomically Thin MoS_2: A New Direct-Gap Semiconductor, Phys. Rev. Lett. **105**, 136805 (2010).

[3] K. F. Mak and J. Shan, Photonics and optoelectronics of 2D semiconductor transition metal dichalcogenides, Nat. Photonics **10**, 216 (2016).

[4] B. Huang, G. Clark, E. Navarro-Moratalla, D. R. Klein, R. Cheng, K. L. Seyler, D. Zhong, E. Schmidgall, M. A. McGuire, D. H. Cobden, W. Yao, D. Xiao, P. Jarillo-Herrero, and X. Xu, Layer-dependent ferromagnetism in a van der Waals crystal down to the monolayer limit, Nature **546**, 270 (2017).

[5] D. Zhong, K. L. Seyler, X. Linpeng, R. Cheng, N. Sivadas, B. Huang, E. Schmidgall, T. Taniguchi, K. Watanabe, M. A. McGuire, W. Yao, D. Xiao, K. C. Fu, and X. Xu, Van der Waals engineering of ferromagnetic semiconductor heterostructures for spin and valleytronics, Sci. Adv. **3**, e1603113 (2017).

[6] C. Gong, L. Li, Z. Li, H. Ji, A. Stern, Y. Xia, T. Cao, W. Bao, C. Wang, Y. Wang, Z. Q. Qiu, R. J. Cava, S. G. Louie, J. Xia, and X. Zhang, Discovery of intrinsic ferromagnetism in two-dimensional van der Waals crystals, Nature **546**, 265 (2017).

[7] Y. Liu and C. Petrovic, Critical behavior of quasi-two-dimensional semiconducting ferromagnet $Cr_2Ge_2Te_6$, Phys. Rev. B **96**, 054406 (2017).

[8] V. Carteaux, F. Moussa, and M. Spiesser, 2D Ising-Like Ferromagnetic Behaviour for the Lamellar $Cr_2Si_2Te_6$ Compound: A Neutron Scattering Investigation, Europhys. Lett. **29**, 251 (1995).

[9] C. Zhang, Y. Gu, L. Wang, L.-L. Huang, Y. Fu, C. Liu, S. Wang, H. Su, J.-W. Mei, X. Zou, and J.-F. Dai, Pressure-Enhanced Ferromagnetism in Layered $CrSiTe_3$ Flakes, Nano Lett. **21**, 7946 (2021).

[10] W. Cai, H. Sun, W. Xia, C. Wu, Y. Liu, H. Liu, Y. Gong, D.-X. Yao, Y. Guo, and M. Wang, Pressure-induced superconductivity and structural transition in ferromagnetic $CrSiTe_3$, Phys.

Rev. B **102**, 144525 (2020).
[11] Q. Dong, J. Pan, S. Li, Y. Fang, T. Lin, S. Liu, B. Liu, Q. Li, F. Huang, and B. Liu, Record-High Superconductivity in Transition Metal Dichalcogenides Emerged in Compressed 2H-TaS_2, Adv. Mater. **34**, 2103168 (2022).
[12] V. Carteaux, D. Brunet, G. Ouvrard, and G. Andre, Crystallographic, magnetic and electronic structures of a new layered ferromagnetic compound $Cr_2Ge_2Te_6$, J. Phys.: Condens. Matter **7**, 69 (1995).
[13] H. Ji, R. A. Stokes, L. D. Alegria, E. C. Blomberg, M. A. Tanatar, A. Reijnders, L. M. Schoop, T. Liang, R. Prozorov, K. S. Burch, N. P. Ong, J. R. Petta, and R. J. Cava, A ferromagnetic insulating substrate for the epitaxial growth of topological insulators, J. Appl. Phys. **114**, 114907 (2013).
[14] N. Wang, H. Tang, M. Shi, H. Zhang, W. Zhuo, D. Liu, F. Meng, L. Ma, J. Ying, L. Zou, Z. Sun, and X. Chen, Transition from Ferromagnetic Semiconductor to Ferromagnetic Metal with Enhanced Curie Temperature in $Cr_2Ge_2Te_6$ via Organic Ion Intercalation, J. Am. Chem. Soc. **141**, 17166–17173 (2019).
[15] D. Bhoi, J. Gouchi, N. Hiraoka, Y. Zhang, N. Ogita, T. Hasegawa, K. Kitagawa, H. Takagi, K. H. Kim, and Y. Uwatoko, Nearly Room-Temperature Ferromagnetism in a Pressure-Induced Correlated Metallic State of the van der Waals Insulator $CrGeTe_3$, Phys. Rev. Lett. **127**, 217203 (2021).
[16] T. Sakurai, B. Rubrecht, L. T. Corredor, R. Takehara, M. Yasutani, J. Zeisner, A. Alfonsov, S. Selter, S. Aswartham, A. U. B. Wolter, B. Büchner, H. Ohta, and V. Kataev, Pressure control of the magnetic anisotropy of the quasi-two-dimensional van der Waals ferromagnet $Cr_2Ge_2Te_6$, Phys. Rev. B **103**, 024404 (2021).
[17] Z. Yu, W. Xia, K. Xu, M. Xu, H. Wang, X. Wang, N. Yu, Z. Zou, J. Zhao, L. Wang, X. Miao, and Y. Guo, Pressure-Induced Structural Phase Transition and a Special Amorphization Phase of Two-Dimensional Ferromagnetic Semiconductor $Cr_2Ge_2Te_6$, J. Phys. Chem. C, **123**, 13885−13891 (2019).
[18] K. Xu, Z. Yu, W. Xia, M. Xu, X. Mai, L. Wang, Y. Guo, X. Miao, and M. Xu, Unique 2D–3D Structure Transformations in Trichalcogenide $CrSiTe_3$ under High Pressure, J. Phys. Chem. C **124**, 15600–15606 (2020).
[19] W. Ge, K. Xu, W. Xia, Z. Yu, H. Wang, X. Liu, J. Zhao, X. Wang, N. Yu, Z. Zou, Z. Yan, L. Wang, M. Xu, and Y. Guo, Raman spectroscopy and lattice dynamical stability study of 2D ferromagnetic semiconductor $Cr_2Ge_2Te_6$ under high pressure, J. Alloy. Compd. **819**, 153368 (2020).
[20] F. Weber, S. Rosenkranz, J.-P. Castellan, R. Osborn, G. Karapetrov, R. Hott, R. Heid, K.-P. Bohnen, and A. Alatas, Electron-Phonon Coupling and the Soft Phonon Mode in $TiSe_2$, Phys. Rev. Lett. **107**, 266401 (2011).
[21] E. Karaca, S. Bağcı, H. M. Tütüncü, H. Y. Uzunok, and G. P. Srivastava, Theoretical investigation of electron-phonon interaction in the orthorhombic phase of Mo_2C, J. Alloy. Compd. **788**, 842 (2019).
[22] X. Liang, S. Zhao, C. Shao, A. Bergara, H. Liu, L. Wang, R. Sun, Y. Zhang, Y. F. Gao, Z. S.

Zhao X. Zhou, J. He, D. Yu, G. Gao, and Y. Tian, First-principles study of crystal structures and superconductivity of ternary YSH_6 and $LaSH_6$ at high pressures, Phys. Rev. B **100**, 184502 (2019).

[23] K. Momma and F. Izumi, VESTA 3 for three-dimensional visualization of crystal, volumetric and morphology data, J. Appl. Crystallogr. **44**, 1272 (2011).

[24] R. Matsumoto, Y. Sasama, M. Fujioka, T. Irifune, M. Tanaka, T. Yamaguchi, H. Takeya, and Y. Takano, Note: Novel diamond anvil cell for electrical measurements using boron-doped metallic diamond electrodes, Rev. Sci. Instrum. **87**, 076103 (2016).

[25] R. Matsumoto, T. Irifune, M. Tanaka, H. Takeya, and Y. Takano, Diamond anvil cell using metallic diamond electrodes, Jpn. J. Appl. Phys. **56**, 05FC01 (2017).

[26] R. Matsumoto, A. Yamashita, H. Hara, T. Irifune, S. Adachi, H. Takeya, and Y. Takano, Diamond anvil cells using boron-doped diamond electrodes covered with undoped diamond insulating layer, Appl. Phys. Express **11**, 053101 (2018).

[27] H. K. Mao, P. M. Bell, J. W. Shaner, and D. J. Steinberg, Specific volume measurements of Cu, Mo, Pd, and Ag and calibration of the ruby R_1 fluorescence pressure gauge from 0.06 to 1 Mbar, J. Appl. Phys. **49**, 3276 (1978).

[28] Y. Akahama and H. Kawamura, High-pressure Raman spectroscopy of diamond anvils to 250 GPa: Method for pressure determination in the multi-megabar pressure range, J. Appl. Phys. **96**, 3748 (2004).

[29] Y. Seto, D. Hamane, T. Nagai, and K. Fujino, Fate of carbonates within oceanic plates subducted to the lower mantle, and a possible mechanism of diamond formation, Phys. Chem. Miner. **35**, 223-229 (2008).

[30] Y. F. Li, W. Wang, W. Guo, C. Y. Gu, H. Y. Sun, L. He, J. Zhou, Z. B. Gu, Y. F. Nie, and X. Q. Pan, Electronic structure of ferromagnetic semiconductor $CrGeTe_3$ by angle-resolved photoemission spectroscopy, Phys. Rev. B **98**, 125127 (2018).

[31] Z. Lin, M. Lohmann, Z. A. Ali, C. Tang, J. Li, W. Xing, J. Zhong, S. Jia, W. Han, S. Coh, W. Beyermann, and J. Shi, Pressure-induced spin reorientation transition in layered ferromagnetic insulator $Cr_2Ge_2Te_6$, Phys. Rev. Mater. **2**, 051004(R) (2018).

[32] Y. Tian, M.J. Gray, H. Ji, R.J. Cava, and K.S. Burch, Magneto-elastic coupling in a potential ferromagnetic 2D atomic crystal, 2D Mater. **3**, 025035 (2016).

[33] Y. Sun, R. C. Xiao, G. T. Lin, R. R. Zhang, L. S. Ling, Z. W. Ma, X. Luo, W. J. Lu, Y. P. Sun, and Z. G. Sheng, Appl. Phys. Lett. **112**, 072409 (2018).

[34] W.-P. Hsieh, P. Zalden, M. Wuttig, A. M. Lindenberg, and W. L. Mao, High-pressure Raman spectroscopy of phase change materials, Appl. Phys. Lett. **103**, 191908 (2013).

[35] (Supplemental material) Ruby fluorescence with cBN is provided online.

[36] R. T. Downs and A. K. Singh, Analysis of deviatoric stress from nonhydrostatic pressure on a single crystal in a diamond anvil cell: The case of monoclinic aegirine, $NaFeSi_2O_6$, J. Phys. Chem. Solids **67**, 1995 (2006).

[37] Z. H. Ni, T. Yu, Y. H. Lu, Y. Y. Wang, Y. P. Feng, and Z. X. Shen, Uniaxial Strain on Graphene: Raman Spectroscopy Study and Band-Gap Opening, ACS Nano **2**, 2301 (2008).

[38] R. Yang, J. Lee, S. Ghosh, H. Tang, R. M. Sankaran, C. A. Zorman, and P. X.-L. Feng, Tuning

Optical Signatures of Single- and Few-Layer MoS_2 by Blown-Bubble Bulge Straining up to Fracture, Nano Lett. **17**, 4568 (2017).

[39] Z. Zhang, L. Li, J. Horng, N. Z. Wang, F. Yang, Y. Yu, Y. Zhang, G. Chen, K. Watanabe, T. Taniguchi, X. H. Chen, F. Wang, and Y. Zhang, Strain-Modulated Bandgap and Piezo-Resistive Effect in Black Phosphorus Field-Effect Transistors, Nano Lett. **17**, 6097 (2017).